

See discussions, stats, and author profiles for this publication at: <https://www.researchgate.net/publication/343659117>

AAS 20-690 STOCHASTIC SPACECRAFT NAVIGATION AND CONTROL IN LIE GROUP SE(3) AROUND SMALL IRREGULAR BODIES

Preprint · August 2020

DOI: 10.13140/RG.2.2.21502.82240

CITATION

1

READS

473

5 authors, including:



Matthew Wittal

NASA

8 PUBLICATIONS 1 CITATION

[SEE PROFILE](#)



Gennaro Mangiacapra

Politecnico di Torino

2 PUBLICATIONS 1 CITATION

[SEE PROFILE](#)



Akhilesh Appakonam

Embry-Riddle Aeronautical University

1 PUBLICATION 1 CITATION

[SEE PROFILE](#)



Morad Nazari

Embry-Riddle Aeronautical University

63 PUBLICATIONS 604 CITATIONS

[SEE PROFILE](#)

Some of the authors of this publication are also working on these related projects:



Spectral Methods for numerical solution of fractional delay differential equations (MATLAB Toolbox) [View project](#)



Set-Theoretic Model Reference Adaptive Control [View project](#)

STOCHASTIC SPACECRAFT NAVIGATION AND CONTROL IN LIE GROUP SE(3) AROUND SMALL IRREGULAR BODIES

Matthew M. Wittal*, Gennaro Mangiacapra†, Akku Appakonam‡,

Morad Nazari§ and Elisa Capello¶

This work presents a novel rigid-body spacecraft navigation and control architecture within the compact special Euclidean group $\text{SE}(3)$ and their tangent bundle $\text{TSE}(3)$ considering stochastic processes in the system. The formulation developed here effectively combines the translational and rotational motions of a rigid-body spacecraft into a single compact set and presents the integration of a stochastic estimator-based control for spacecraft motion in a highly nonlinear, irregular-shape small-body environment using a novel $\text{TSE}(3)$ framework. The theoretical navigation and control architecture created here is studied for the case of hovering problem around the Saturnian moon Pan and the asteroid Bennu. The effectiveness of the estimator and controller are examined in the simulations. Furthermore, the augmentation of the stochastic estimator and the almost-globally asymptotically stabilizing controller is proved to be a reliable, functional approach for spacecraft navigation and control in highly perturbed environments near small bodies with irregular shapes.

INTRODUCTION

Spacecraft can be adequately approximated as rigid bodies defining the spacecraft motion as a six degrees of freedom body with translational (orbital) and rotational (attitude) motions, while this assumption excludes the possibility of taking flexible body dynamics into account. Different representations can be found in the literature for dynamics. Particularly, the spacecraft translational motion can be formulated and propagated using several type of formulation such as Cowell, Encke, Clohessy-Wiltshire, equinoctial elements or unified state model [1–3]. Since the spacecraft trajectory is mainly influenced by the gravitational attraction of other celestial bodies, the aforementioned methods take advantage of the orbital mechanics to improve the stability and accuracy of the dynamics propagation.

The spacecraft kinematics model depends on the attitude parameterization set used for the attitude motion, which is often defined by three or four parameters. The discuss and mathematical formulation of the commonly used spacecraft attitude representations can be found in [4, 5], for instance. These attitude parameterization sets can be minimal three-parameter sets defined in 3-dimensional Euclidean space \mathbb{R}^3 (principal rotation, classical Rodrigues parameters, modified Rodrigues parameters, Euler angles), or four-parameter set defined on the 3-sphere S^3 (quaternions). Alternatively, rigid body attitude can be represented using the direction cosine matrix (rotation matrix) defined on the special orthogonal group $\text{SO}(3)$.

Conventionally, the analysis of the orbital and attitude dynamics of the spacecraft are conducted separately resulting in separate control laws for attitude and translational motion. However, as clearly discussed in several references such as [4, 6, 7], the coupling between the translational dynamics and rotation of the spacecraft should be considered in spacecraft dynamics analysis and control design. The simultaneous modeling of

*Graduate Student, Aerospace Engineering Department, Embry-Riddle Aeronautical University, Daytona Beach, FL 32114, USA & Scientist, NASA Kennedy Space Center, FL 32899, USA

†Graduate Student, Department of Mechanical and Aerospace Engineering, Politecnico di Torino, Torino 10129, Italy

‡Graduate Student, Aerospace Engineering Department, Embry-Riddle Aeronautical University, Prescott, AZ 86301, USA

§Assistant Professor, Aerospace Engineering Department, Embry-Riddle Aeronautical University, Daytona Beach, FL 32114, USA

¶Assistant Professor, Department of Mechanical and Aerospace Engineering, Politecnico di Torino, CNR-IEIIT, Torino 10129, Italy

spacecraft orbital/attitude dynamics using special Euclidean group $\text{SE}(3)$ is advantageous since it considers the coupling between translational and rotational dynamics. Such coupling can be due to gravity gradient forces and torques in highly nonlinear gravity fields, attitude-dependent forces and torques due to drag and solar radiation pressure, spacecraft rendezvous and proximity operations, or spacecraft hovering over small bodies, for instance. This coupling has been considered in dynamic analysis and control design of rigid body or spacecraft, as in [8–12] and results in accurate, viable results for the rigid body and rigid-body spacecraft motion.

In real world applications, navigation is a crucial part of any guidance, navigation, and control (GN&C) system and it enables the correct estimation of the spacecraft state based on the input of sensor measurements. The on-board instruments such as inertial measurement unit, gyroscopes, accelerometers, etc. have limited accuracy and are usually characterized by a certain degree of uncertainty. These uncertainties can arise not only because of the instruments but also from electrical components, communication systems, or external disturbances such as solar radiation pressure, and result in inaccuracies in the measurements. For the reason mentioned above, the states of the system changes over time as stochastic processes and the need for using an estimators, such as the Kalman-type filters, capable of handling stochastic sources arises.

Although, as mentioned above, control problem on $\text{SE}(3)$ for space applications has been extensively studied, the navigation problem is not usually analyzed for this particular field in literature. Navigation tools based on $\text{SE}(3)$ have been increasingly developed in the past decade; several works have studied estimator design using the extended Kalman filter (EKF) [13] or the unscented Kalman filter (UKF) [14, 15] on $\text{SE}(3)$. Moreover, from the literature, it can be seen how these estimators are efficient, although formulation development of the filter design in $\text{SE}(3)$ is mathematically more complex than filter algorithms developed in Euclidean space. This may have been solved in specific cases by the use of a modified discrete EKF (D-EKF) or of an UKF, as applied in robotics [16]. Other recent efforts, such as those by [17], have laid a solid foundation on stochastic estimation in Lie groups on which to build this work.

In this paper, a novel spacecraft navigation and control system on $\text{TSE}(3)$ has been developed. The novelty of the approach described herein is the integration of various components of $\text{SE}(3)$, $\text{TSE}(3)$, and stochastic estimation in Lie Groups into a single applicable method to spacecraft navigation and control. The algorithm in this work results in a more accurate dynamical analysis, is singularity free, and does not encounter any unwinding issues that arise when quaternions are used. Additionally, it is a coupled formulation that enables the design a single control law that accurately takes into account both translational and rotational motion. The gravitational interaction between the spacecraft rigid body and the small irregular central body is modeled according to [18]. The starting point is the design of a mathematical formulation that is able to describe a dynamic system on $\text{TSE}(3)$ characterized by stochastic processes. Subsequently, the navigation and control system are designed. Starting from the work in [19] the UKF filter is protracted to the tangent bundle $\text{TSE}(3)$. The controller is based on the algorithm given in [9], where a control law suitable for stabilization problem is extended to tracking problem. The efficacy of this methodology is shown in applications around two small irregular bodies, and is extensible to any other small body. The first example is a tracking problem around the Saturnian moon Pan, and is representative of an observation mission around this unknown celestial object. The second one is an hovering problem around the Near-Earth Object (NEO) Bennu, and is representative of a pre-landing phase that focuses on navigating to a specific point of interest. The results are presented in terms of the state estimator accuracy, controller effort, and convergence time as well as orbit coverage and the overall flexibility of this approach.

PRELIMINARIES AND PROBLEM STATEMENT

Lie group $\text{SE}(3)$ and its Lie algebra $\mathfrak{se}(3)$

The spacecraft configuration is defined by 6 degrees of freedom, 3 of which related to the location of its center of mass and the other 3 related to its attitude. According to [20,21], the configuration space of a rigid-body spacecraft is the Lie group $\text{SE}(3)$. This is a smooth manifold obeying the group properties (closure under multiplication, identity, associativity, and invertability) with the additional condition that the group operations are differentiable. The $\text{SE}(3)$ is defined as the semi-direct product of \mathbb{R}^3 and $\text{SO}(3)$, i.e. $\text{SE}(3) = \mathbb{R}^3 \times \text{SO}(3)$,

or, equivalently,

$$\text{SE}(3) = \left\{ g \mid g = \begin{bmatrix} R & \mathbf{r} \\ 0_{1 \times 3} & 1 \end{bmatrix}, R \in \text{SO}(3), \mathbf{r} \in \mathbb{R}^3 \right\} \quad (1)$$

where

$$\text{SO}(3) = \{ R \in \mathbb{R}^{3 \times 3} \mid R^T R = I_3, \det(R) = +1 \} \quad (2)$$

where R is the rotation matrix from the body frame to the inertial frame, \mathbf{r} is the position vector from the origin of the inertial frame to the center of mass of the rigid body, and I_3 is the 3×3 identity matrix. The smoothness of the matrix Lie group implies the existence of a single tangent space at each point. Particularly, the tangent space at the identity element of the group is referred to as Lie algebra [22], also denoted as

$$\mathfrak{se}(3) = \left\{ \mathbb{V}^\vee = \begin{bmatrix} \boldsymbol{\omega}^\times & \mathbf{v} \\ 0_{1 \times 3} & 0 \end{bmatrix}, \boldsymbol{\omega}^\times \in \mathfrak{so}(3), \mathbf{v} \in \mathbb{R}^3 \right\} \quad (3)$$

where $(\cdot)^\vee$ indicates the wedge map, i.e. $(\cdot)^\vee : \mathbb{R}^6 \rightarrow \mathfrak{se}(3)$ applied to the vector $\mathbb{V} = [\boldsymbol{\omega}^T, \mathbf{v}^T]^T$; $\mathfrak{so}(3)$ is the set of 3 by 3 skew symmetric matrices such that $\boldsymbol{\omega}^\times$ can be defined in terms of the components of the angular velocity vector $\boldsymbol{\omega} \in \mathbb{R}^3$. According to [23], given the vector $\boldsymbol{\Omega} = [\Omega_1, \Omega_2, \Omega_3]^T$, the cross map $(\cdot)^\times : \mathbb{R}^3 \rightarrow \mathfrak{so}(3)$ is defined as

$$\boldsymbol{\Omega}^\times = \begin{bmatrix} 0 & -\Omega_3 & \Omega_2 \\ \Omega_3 & 0 & -\Omega_1 \\ -\Omega_2 & \Omega_1 & 0 \end{bmatrix} \quad (4)$$

From the definition of Lie group $\text{SE}(3)$ and its Lie algebra $\mathfrak{se}(3)$, the geometric link between the two formulations can be understood. The Lie algebra can be considered as a linearization of the Lie group, near the identity element [24]. The nonlinear structure of the Lie group can be translated in a complicated mathematical structure, which makes it difficult to study with conventional mathematical tools. The important feature of the Lie algebra is that it is a linear vector space, thus it can be studied using the tools developed in linear algebra. However, the extraction of the $\text{SE}(3)$ properties from its Lie algebra opens the possibility to several scientific applications [25].

The exponential map $\exp : \mathfrak{se}(3) \rightarrow \text{SE}(3)$ allows to transfer elements of the Lie algebra to the Lie group which, intuitively, can be interpreted as a wrapping operation, from the tangent plane onto the manifold. Formally, it is a local diffeomorphism from a neighborhood of zero in $\mathfrak{se}(3)$ onto a neighborhood of the identity element in $\text{SE}(3)$ [23]. The exponential coordinates are defined as

$$\boldsymbol{\xi} = \begin{bmatrix} \boldsymbol{\Theta} \\ \mathbf{p} \end{bmatrix} \in \mathbb{R}^6, \quad (5)$$

where $\boldsymbol{\Theta} \in \mathbb{R}^3$ is the product of eigenaxis (principal axis) and eigenangle (principal angle) of rotation, i.e. $\boldsymbol{\Theta} = \theta \mathbf{e}$ and $\|\boldsymbol{\Theta}\| = \theta$, and $\mathbf{p} \in \mathbb{R}^3$ represent the translational vector components. With the previous definition, the configuration g is obtained via exponential map $\exp : \mathfrak{se}(3) \rightarrow \text{SE}(3)$ as

$$g = \exp(\boldsymbol{\xi}^\vee) = \sum_{n=0}^{\infty} \frac{1}{n!} (\boldsymbol{\xi}^\vee)^n, \quad (6)$$

which can be written as [26]

$$g = \begin{bmatrix} R(\boldsymbol{\Theta}) & S(\boldsymbol{\Theta})\mathbf{p} \\ 0 & 1 \end{bmatrix} \in \text{SE}(3), \quad (7)$$

where $R(\boldsymbol{\Theta}) \in \text{SO}(3)$ is the rotation matrix from body frame to the inertial frame and is obtained via Rodrigues formula as

$$R(\boldsymbol{\Theta}) = \exp(\boldsymbol{\Theta}^\times) = I + \frac{\sin \theta}{\theta} \boldsymbol{\Theta}^\times + \frac{1 - \cos \theta}{\theta^2} (\boldsymbol{\Theta}^\times)^2, \quad (8)$$

and

$$S(\Theta) = I + \frac{1 - \cos \theta}{\theta^2} \Theta^\times + \frac{\theta - \sin \theta}{\theta^3} (\Theta^\times)^2. \quad (9)$$

Note that the inverse of the exponential map is the logarithmic map $\log : \text{SE}(3) \rightarrow \mathfrak{se}(3)$ which can be interpreted as an unwrapping operation. The exponential coordinates can be obtained via logarithmic map as

$$\xi^\vee = \log_{\text{SE}(3)}(g) \quad (10)$$

System formulation on SE(3)

The rigid body kinematic and kinetic equations of motion are given as

$$\dot{g} = g \mathbb{V}^\vee, \quad (11)$$

$$\dot{\mathbb{V}} = \mathbb{I}^{-1} \text{ad}_\mathbb{V}^* \mathbb{I} \mathbb{V} + \mathbb{I}^{-1} (\mathbf{u}_g + \mathbf{u}_c),$$

where g , defined in Eq. (1), represents the rigid body configuration, $\mathbb{V} = [\boldsymbol{\omega}^T, \mathbf{v}^T]^T$ expresses the rigid body augmented velocity vector, $\mathbf{u}_g \in \mathbb{R}^6$ denotes the total external inputs such as gravitational effects, and $\mathbf{u}_c \in \mathbb{R}^6$ is the control input (control moment and control force). The complete state is thus represented by $(g, \mathbb{V}) \in \text{SE}(3) \times \mathbb{R}^6 = \text{TSE}(3)$, the tangent bundle of SE(3). In this framework, both the attitude and the linear position are considered simultaneously. This allows to design an estimation algorithm and a control system in TSE(3), which is more versatile and more accurate than the standard decoupled procedures. This formulation advantages the coupling of the translational and the rotational motions, as the spacecraft dynamical system. In Eq. (11), the inertia tensor in SE(3) is represented by

$$\mathbb{I} = \begin{bmatrix} J & 0_{3 \times 3} \\ 0_{3 \times 3} & mI_3 \end{bmatrix} \in \mathbb{R}^6 \quad (12)$$

where J is the moment of inertia about the center of mass, and m is the mass of the system. Moreover, the co-adjoint operator is defined as

$$\text{ad}_\mathbb{V}^* = \text{ad}_\mathbb{V}^T = \begin{bmatrix} -\boldsymbol{\omega}^\times & -\mathbf{v}^\times \\ 0_{3 \times 3} & -\boldsymbol{\omega}^\times \end{bmatrix}, \quad (13)$$

where the adjoint operator $\text{ad}_\mathbb{V}$ is

$$\text{ad}_\mathbb{V} = \begin{bmatrix} \boldsymbol{\omega}^\times & 0_{3 \times 3} \\ -\mathbf{v}^\times & -\boldsymbol{\omega}^\times \end{bmatrix}. \quad (14)$$

From an intuitive point of view, this operator allows to transform a tangent vector from the tangent space around one element to the tangent space around another one.

Dynamics of Spacecraft Hovering Near Small Bodies

For many small bodies, the asymmetric distribution of mass becomes a more significant element in the dynamics than in their larger counterparts such as Earth, Jupiter, or their major moons. For rigid body dynamics, the torque on the moment of the spacecraft caused by the asymmetry is an additional factor that must be considered. The gravity potential of second degree and order of the celestial body is [27]

$$U = \frac{\mu}{\|\boldsymbol{\rho}\|} + \frac{\mu}{\|\boldsymbol{\rho}\|^3} \left(-\frac{C_{20}}{2} + 3C_{22} \right) + \frac{3\mu}{\|\boldsymbol{\rho}\|^4} \left(-2C_{22}\hat{\mathbf{r}} \cdot \hat{\mathbf{J}} + \left(\frac{C_{20}}{2} - C_{22} \right) \hat{\mathbf{r}} \cdot \hat{\mathbf{K}} \right), \quad (15)$$

where $\boldsymbol{\rho}$ is the position vector of an arbitrary point on the spacecraft in the Body-Centered Inertial (BCI) frame, i.e. $\mathbf{r} = \frac{1}{m} \int_B \boldsymbol{\rho} dm$, $(\hat{\mathbf{I}}, \hat{\mathbf{J}}, \hat{\mathbf{K}})$ is the unit basis of the BCI frame, and the second degree and order coefficients are [28–30]

$$C_{20} = -J_2 = \frac{1}{5r_o^2} \left(\gamma^2 - \frac{\alpha^2 + \beta^2}{2} \right), \quad C_{22} = \frac{1}{20r_o^2} (\alpha^2 - \beta^2) \quad (16)$$

where $\alpha = 1$, $\beta = \frac{l_2}{l_1}$, and $\gamma = \frac{l_3}{l_1}$ are normalized parameterizations of the dimensions of any given triaxial ellipsoid with major axes $l_1 > l_2 > l_3$.

Taking the partial derivative of the gravity potential U in Eq.(15) with respect to ρ , integrating over the body of the spacecraft, and keeping only the terms up to order $1/\|\rho\|^4$, the gravity gradient force applied to the spacecraft expressed in Spacecraft Body Fixed (SBF) coordinates is approximated as

$$\mathbf{F}_g = R^T \int_{\mathcal{B}} \frac{\partial U}{\partial \rho} dm = R^T (\mathbf{F}_{g_1} + \mathbf{F}_{g_2}), \quad (17)$$

where R is the rotation matrix from the SBF frame to the BCI frame,

$$\mathbf{F}_{g_1} = -m \frac{\mu}{\|\mathbf{r}\|^3} \left(1 + \frac{3}{m\|\mathbf{r}\|^2} \left[J + \frac{1}{2} \left(\text{tr}(J) - \frac{5}{\|\mathbf{r}\|^2} \mathbf{r}^T R J R^T \mathbf{r} \right) I_3 \right] \right) \mathbf{r}, \quad (18)$$

\mathbf{r} denotes the position of the center of mass of spacecraft with respect to the center of mass of the central body expressed in the BCI frame, and

$$\mathbf{F}_{g_2} = \frac{m\mu}{\|\mathbf{r}\|^4} \left(\begin{bmatrix} \left(\frac{3}{2}C_{20} - 9C_{22}\right) (\hat{\mathbf{r}} \cdot \hat{\mathbf{I}}) \\ \left(\frac{3}{2}C_{20} - 21C_{22}\right) (\hat{\mathbf{r}} \cdot \hat{\mathbf{J}}) \\ \left(\frac{9}{2}C_{20} - 15C_{22}\right) (\hat{\mathbf{r}} \cdot \hat{\mathbf{K}}) \end{bmatrix} + \frac{15}{\|\mathbf{r}\|} \left(\left(-\frac{C_{20}}{2} + C_{22}\right) \hat{\mathbf{r}} \cdot \hat{\mathbf{K}} + 2C_{22}\hat{\mathbf{r}} \cdot \hat{\mathbf{J}} \right) \hat{\mathbf{r}} \right) \quad (19)$$

which is an alternative way of representation to what is shown in [18], and where $\hat{\mathbf{I}}$, $\hat{\mathbf{J}}$ and $\hat{\mathbf{K}}$ are principle direction vectors in the PCPF frame. The gravity gradient torque on the rigid-body spacecraft due to the gravitational field of the central body is expressed as

$$\mathbf{M}_g = 3 \frac{\mu}{\|\mathbf{r}\|^5} ((R^T \mathbf{r})^\times J R^T \mathbf{r}) \quad (20)$$

Therefore, the total augmented external effect given in Eq. (11) is $\mathbf{u}_g = [\mathbf{F}_g^T, \mathbf{M}_g^T]^T$, where the gravitational force and moment are given in Eqs. (17) and (20), respectively.

STOCHASTIC PROCESSES, FILTER, AND CONTROL DESIGN ON THE LIE GROUP

Stochastic processes on Lie groups and system formulation

The mathematical model employed for the control and state estimation is usually developed in the Euclidean space, which is an affine space and, by definition, it is a geometric structure based on the vectorial space [22]. When the mathematical modeling is performed in Euclidean space, it is only possible to deal with uncertainties using an additive approach. This restriction is removed by formulating the problem on the nonlinear manifold of $\text{SE}(3)$. However, when the model is developed in $\text{SE}(3)$, uncertainties and stochastic processes cannot be formulated using the conventional mathematical models that are commonly used in the Euclidean space. This is due to the fact that $\text{SE}(3)$ is a nonlinear manifold and not a vectorial space [31]. In this paper, the formulation covered in [14] is used to accommodate a stochastic process in the model. Since the source of noise is assumed to be in vector space, the exponential map $\exp(\cdot)$ is used to map it into $\text{SE}(3)$ as

$$\chi_\eta = \bar{\chi}_\eta \exp(\eta^\vee) \quad \eta \sim \mathcal{N}(0, P) \quad (21)$$

where χ_η is the noise in $\text{SE}(3)$ and $\mathcal{N}(0, P)$ denotes the Gaussian distribution in Euclidean space with zero mean and covariance matrix $P \in \mathbb{R}^{6 \times 6}$. In Eq. (21), post multiplication by $\bar{\chi}_\eta$ causes the original Gaussian ξ of the Lie algebra to center at $\bar{\chi}_\eta \in \text{SE}(3)$. The symbols χ_η and $\bar{\chi}_\eta$ represent a small perturbation with covariance P and a large source of noise, respectively.

The estimation phase is a necessary step to overcome the stochastic nature of the real system. Generally, it is possible to consider two types of noise: one dependent on the system and another dependent on the measurements of the sensors. If the nonlinear system dynamic plant is represented by the equations

$$\dot{\mathbf{x}}(t) = \mathbf{f}[\mathbf{x}(t), \mathbf{u}(t), t] \quad (22)$$

$$\mathbf{y}(t) = \mathbf{h}[\mathbf{x}(t), \mathbf{u}(t), t]$$

then, the real system plant affected by the two types of noise is defined as

$$\begin{aligned}\dot{\mathbf{x}}(t) &= \mathbf{f}[\mathbf{x}(t), \mathbf{u}(t), t] + G[\mathbf{x}(t), t]\boldsymbol{\eta}(t) \\ \mathbf{y}(t) &= \mathbf{h}[\mathbf{x}(t), \mathbf{u}(t), t] \\ \mathbf{z}(t) &= \mathbf{y}(t) + \boldsymbol{\zeta}(t)\end{aligned}\tag{23}$$

where $\mathbf{f}[\cdot]$ is the nonlinear state transition function, $\mathbf{h}[\cdot]$ is the nonlinear measurement function, $G[\cdot]$ is the input noise matrix, \mathbf{y} is the noise-free measurement vector, \mathbf{z} the real measurement vector, \mathbf{x} denotes the system state, and \mathbf{u} denotes the system input, both gravitational and control. This is the system equation form that best accommodates the application of Kalman filter theory and that is conventionally used in the aerospace sector [32]. The process noise $\boldsymbol{\eta}(t)$ statistics, the sensor noise $\boldsymbol{\zeta}(t)$ statistics, and the joint sensor-process noise statistics are expressed through covariance matrices based on the knowledge of the equipment used on-board.

The state of the system $\mathbf{x} = (g, \mathbb{V})$ is in TSE(3) and hence the model expressed in Eq. (23) is not trivial. The attitude and position part of the state are defined on SE(3), while the velocities are expressed in the Euclidean space. Although in literature many application of estimation techniques can be found, none of them take into account a state vector defined on TSE(3). For this reason a novel augmented formulation is introduced in this work, which is in agreement with the system dynamics presented above. The nonlinear state transition function $\mathbf{f}[\cdot]$ can be divided into

$$\begin{aligned}\mathbf{f}_1[\mathbf{x}(t), \mathbf{u}(t), t] &= g\mathbb{V}^\vee \\ \mathbf{f}_2[\mathbf{x}(t), \mathbf{u}(t), t] &= \mathbb{I}^{-1}\text{ad}_{\mathbb{V}}^*\mathbb{I}\mathbb{V} + \mathbb{I}^{-1}\mathbf{u},\end{aligned}\tag{24}$$

where $\mathbf{f}_1 \in \text{SE}(3)$ and $\mathbf{f}_2 \in \mathbb{R}^6$. In order to complete the model, the nonlinear measurement function $\mathbf{h}[\cdot]$ is also introduced. It is assumed that the system output components are the principal angles of rotation, the translational vector components, the angular velocity and the translational velocity:

$$\mathbf{y} = [\Theta^T, \mathbf{r}^T, \boldsymbol{\omega}^T, \mathbf{v}^T]^T \in \mathbb{R}^{12}\tag{25}$$

As done for the state, also the output is divided in two parts, the first one takes into account the attitude and the translational motion of the spacecraft, while the second one includes the velocities. The measurement functions are then defined as

$$\begin{aligned}\mathbf{h}_1[\mathbf{x}(t), \mathbf{u}(t), t] &= (\log_{\text{SE}(3)}(g))^\dagger \in \mathbb{R}^6 \\ \mathbf{h}_2[\mathbf{x}(t), \mathbf{u}(t), t] &= \mathbb{V} \in \mathbb{R}^6\end{aligned}\tag{26}$$

where the symbol $(\cdot)^\dagger$ denotes the unwedge operator. Finally the measurement vector is affected by the noise and its components are denoted with the subscript "m" that highlights the fact that they are measured.

$$\mathbf{z} = [\Theta_m^T, \mathbf{r}_m^T, \boldsymbol{\omega}_m^T, \mathbf{v}_m^T]^T \in \mathbb{R}^{12}\tag{27}$$

In agreement with Eq. (21), the process and the measurement noises are assumed to be Gaussian white-noise processes. In addition, they are assumed to be uncorrelated and thus the second order joint central moment, i.e. the covariance, is zero.

$$E\{\boldsymbol{\eta}(t)\} = 0 \quad E\{\boldsymbol{\eta}(t)\boldsymbol{\eta}(t)^T(t+\tau)\} = Q \quad \boldsymbol{\eta} \sim \mathcal{N}(0, Q)\tag{28}$$

$$E\{\boldsymbol{\zeta}(t)\} = B \quad E\{\boldsymbol{\zeta}(t)\boldsymbol{\zeta}(t)^T(t+\tau)\} = R \quad \boldsymbol{\zeta} \sim \mathcal{N}(B, R)\tag{29}$$

$$E\{\boldsymbol{\zeta}(t)\boldsymbol{\eta}(t)^T(t+\tau)\} = 0\tag{30}$$

where $Q \in \mathbb{R}^{12 \times 12}$ is the process noise covariance matrix, $R \in \mathbb{R}^{12 \times 12}$ is the measurement noise covariance matrix and $B \in \mathbb{R}^{12 \times 12}$ contains the biases. In order to make the following derivations easier, the measurement noise $\boldsymbol{\eta} \in \mathbb{R}^{12}$ and the process noise $\mathbf{v} \in \mathbb{R}^{12}$ are, for convenience, written as

$$\begin{aligned}\boldsymbol{\eta} &= [\boldsymbol{\eta}_{\Theta}^T, \boldsymbol{\eta}_{\mathbf{p}}^T, \boldsymbol{\eta}_{\omega}^T, \boldsymbol{\eta}_{\mathbf{v}}^T]^T = [\boldsymbol{\eta}_g^T, \boldsymbol{\eta}_{\mathbb{V}}^T]^T \\ \boldsymbol{\zeta} &= [\boldsymbol{\zeta}_{\Theta}^T, \boldsymbol{\zeta}_{\mathbf{p}}^T, \boldsymbol{\zeta}_{\omega}^T, \boldsymbol{\zeta}_{\mathbf{v}}^T]^T = [\boldsymbol{\zeta}_g^T, \boldsymbol{\zeta}_{\mathbb{V}}^T]^T\end{aligned}\tag{31}$$

where $\boldsymbol{\eta}_g, \boldsymbol{\eta}_{\mathbb{V}}, \boldsymbol{\zeta}_g, \boldsymbol{\zeta}_{\mathbb{V}} \in \mathbb{R}^6$ denote the measurement and process noises related to the part of the states in SE(3) and Euclidean space, respectively. Also, $\boldsymbol{\eta}_{\Theta}, \boldsymbol{\eta}_{\mathbf{p}}, \boldsymbol{\eta}_{\omega}, \boldsymbol{\eta}_{\mathbf{v}}, \boldsymbol{\zeta}_{\Theta}, \boldsymbol{\zeta}_{\mathbf{p}}, \boldsymbol{\zeta}_{\omega}, \boldsymbol{\zeta}_{\mathbf{v}} \in \mathbb{R}^3$ are the measurement and process noises related to the principal angle, position, angular and translational velocities. According to the previously defined quantities, the stochastic system defined in Eq. (23) can be written on TSE(3) as

$$\begin{aligned}\dot{\mathbf{x}}(t) &: \begin{cases} \dot{g} = \chi_{\boldsymbol{\eta}_g} g \mathbb{V}^{\vee} \\ \dot{\mathbb{V}} = \mathbb{I}^{-1} \text{ad}_{\mathbb{V}}^* \mathbb{I} \mathbb{V} + \mathbb{I}^{-1} \mathbf{u}_i(t) + \boldsymbol{\eta}_{\mathbb{V}}(t) \end{cases} \\ \mathbf{y}(t) &= [(\log_{\text{SE}(3)}(g))^T, \mathbb{V}^T]^T \\ \mathbf{z}(t) &= \mathbf{y}(t) + \boldsymbol{\zeta}(t)\end{aligned}\tag{32}$$

where the process noise related to g is expressed according to Eq.(21) and the dependence on time is omitted for the readability of the equations. Since an input noise matrix as in Eq.(23) cannot be highlighted in TSE(3), the nonlinear state and measurement functions will be denoted as $\mathbf{f}[\mathbf{x}(t), \mathbf{u}(t), t, \boldsymbol{\eta}(t)]$, $\mathbf{h}[\mathbf{x}(t), \mathbf{u}(t), t, \boldsymbol{\zeta}(t)]$. This formulation will be employed in the description of the UKF steps described in the subsequent section. As can be seen, the two stochastic processes are treated differently, specifically in the way in which they affect the system. The measurement noise and the noise that characterizes \mathbb{V} can be simply added since both \mathbf{z} and \mathbb{V} are in the Euclidean space. For the part of the state defined in SE(3), it is possible to find the results shown in Eq.(36) using the properties of the maps \exp and $\log_{\text{SE}(3)}$. Particularly, once g is mapped in $\mathfrak{se}(3)$ it is possible to simply add the noise:

$$\begin{aligned}\chi_{\boldsymbol{\eta}_g} g &= \bar{\chi}_{\boldsymbol{\eta}_g} \exp(\boldsymbol{\eta}_g^{\vee}) g \\ &= \bar{\chi}_{\boldsymbol{\eta}_g} \exp(\boldsymbol{\eta}_g^{\vee}) \exp(\log_{\text{SE}(3)}(g)) \\ &= \bar{\chi}_{\boldsymbol{\eta}_g} \exp(\boldsymbol{\eta}_g^{\vee} + \log_{\text{SE}(3)}(g)) \\ &= \bar{\chi}_{\boldsymbol{\eta}_g} \exp(\boldsymbol{\eta}_g^{\vee} + \boldsymbol{\xi}^{\vee})\end{aligned}\tag{33}$$

Unscented Kalman Filter design on TSE(3)

On the basis of the system definition provided in Eq. (36), the state estimation is performed using the UKF which, among different Kalman filters, has become the most prevalent alternative for nonlinear systems. This filter takes into account the system nonlinearities better than any other Kalman filter developed so far, and it also avoids linearization errors that are common when the EKF approach is used [16]. In addition, the UKF spares the computation of the Jacobians. This allows this algorithm to be versatile and favorable for fast hardware implementation [15]. The filter implementation is based on that given in [19], where an innovative UKF technique on manifolds was introduced. However, it has been extended to handle a system defined on TSE(3).

In general, the EKF-based approaches approximate the state distribution with a Gaussian distribution, which is propagated through the linearized system. This procedure can lead to large errors and a divergent filter. The UKF, instead, handles the problem with a deterministic sampling approach. In the UKF, the Gaussian state distribution is represented by a set of sample points that completely capture the mean and covariance of the distribution. These points are known as sigma points σ and are propagated through the nonlinear dynamics with the purpose of capturing the *a posteriori* mean and covariance with high accuracy. As opposed to the UKF method, the EKF approach is only capable of achieving a first-order accuracy due to the linearization [33].

The UKF algorithm is recursive and is repeated N times, where N denotes the number of samples. It is characterized by two main phases: a) prediction in which an intermediate estimate state $\hat{\mathbf{x}}(k+1|k)$ and state error covariance matrix $P(k+1|k)$ are obtained, propagating $\hat{\mathbf{x}}(k|k)$ using the known *a priori* mathematical model of the system and b) the correction in which the predictions are corrected on the basis of the difference between the predicted and the measured output. In the UKF design here, the variables related to the states and the noise are indicated with the letters d and q , respectively. The dimensions of the uncertain states and noise are both equal to twelve. The sigma point weights are introduced as

$$\begin{aligned}\lambda_d &= (\alpha^2 - 1)d & \lambda_q &= (\alpha^2 - 1)q \\ W_{d,j} &= \frac{1}{2(d + \lambda_d)} & W_{q,j} &= \frac{1}{2(q + \lambda_q)} \\ W_{d,m} &= \frac{\lambda_d}{\lambda_d + d} & W_{q,m} &= \frac{\lambda_q}{\lambda_q + q} \\ W_{d,c} &= \frac{\lambda_d}{\lambda_d + d} + 3 - \alpha^2 & W_{q,c} &= \frac{\lambda_q}{\lambda_q + q} + 3 - \alpha^2\end{aligned}\tag{34}$$

where α denotes the spread of the sigma points around the mean, and usually has a value between 10^{-5} and 1, λ_d and λ_q are constant, and W denotes the sigma point weights. Since the system states are on TSE(3), a retraction function $\varphi(\cdot) : \mathbb{R}^{12} \rightarrow \text{TSE}(3)$ is introduced, which is a smooth, arbitrarily-chosen function that encodes the mean and covariance noise on the Lie group. The retraction function introduced here is also divided into two parts to manage the augmented state:

$$\varphi(t) : \begin{cases} \varphi_g = g \exp(\sigma^\vee) \\ \varphi_{\mathbb{V}} = \mathbb{V} + \sigma \end{cases}\tag{35}$$

The inverse retraction function $\varphi^{-1} : \text{TSE}(3) \rightarrow \mathbb{R}^{12}$ is

$$\varphi^{-1}(t) : \begin{cases} \varphi_g^{-1} = \log_{\text{TSE}(3)}(\hat{g}^{-1}g) \\ \varphi_{\mathbb{V}}^{-1} = \hat{\mathbb{V}} - \mathbb{V} \end{cases}\tag{36}$$

Prediction: Given the current optimal estimated state $\hat{\mathbf{x}}(k|k)$, the mean state is propagated with zero noise. The a posteriori state prediction can be computed as

$$\hat{\mathbf{x}}(k+1|k) = \mathbf{f}[\hat{\mathbf{x}}(k|k), \mathbf{u}(k), t, \mathbf{0}]\tag{37}$$

In order to obtain the *a posteriori* error covariance matrix of the state prediction error, two different components are considered: The first one is based on the states computed without noise and with the sigma points σ_1 that depend on the state error covariance matrix. The second contribution depends on the process noise covariance matrix and is computed with the sigma points σ_2 and with the noise. These sigma points are computed as

$$\begin{aligned}\sigma_{1,j}(k+1) &= \text{col}(\sqrt{(d + \lambda_d)P(k|k)})_j & j &= 1, \dots, d \\ \sigma_{1,j}(k+1) &= -\text{col}(\sqrt{(d + \lambda_d)P(k|k)})_{j-d} & j &= d+1, \dots, 2d \\ \sigma_{2,j}(k+1) &= \text{col}(\sqrt{(q + \lambda_q)Q})_j & j &= 1, \dots, q \\ \sigma_{2,j}(k+1) &= -\text{col}(\sqrt{(q + \lambda_q)Q})_{j-d} & j &= q+1, \dots, 2q\end{aligned}\tag{38}$$

where $\text{col}(\cdot)_j$ denotes the j -th column of the matrix (\cdot) . The states computed with the sigma points are

$$\mathbf{x}_{\sigma_1} = f[\varphi(\hat{\mathbf{x}}(k|k), \sigma_{j,1}(k+1)), \mathbf{u}(k), t, \mathbf{0}] \quad j = 1, \dots, 2d\tag{39}$$

$$\mathbf{x}_{\sigma_2} = f[\varphi(\hat{\mathbf{x}}(k|k), \boldsymbol{\sigma}_{2,j}(k+1)), \mathbf{u}(k), t, \boldsymbol{\sigma}_{2,j}] \quad j = 1, \dots, 2q \quad (40)$$

The states can be retracted back into \mathbb{R}^{12} with the inverse retraction function, i.e.

$$\boldsymbol{\sigma}_{1,new}(k+1) = \varphi^{-1}(\hat{\mathbf{x}}(k+1|k), \mathbf{x}_{\sigma_1}) - \sum_{j=1}^{2d} W_{d,j} \varphi^{-1}(\hat{\mathbf{x}}(k+1|k), \mathbf{x}_{\sigma_1}) \quad (41)$$

$$\boldsymbol{\sigma}_{2,new}(k+1) = \varphi^{-1}(\hat{\mathbf{x}}(k+1|k), \mathbf{x}_{\sigma_2}) - \sum_{j=1}^{2q} W_{q,j} \varphi^{-1}(\hat{\mathbf{x}}(k+1|k), \mathbf{x}_{\sigma_2}) \quad (42)$$

Finally, the state error covariance matrix is computed as

$$P(k+1|k) = P^{(1)}(k+1|k) + P^{(2)}(k+1|k) \quad (43)$$

where

$$\begin{aligned} P^{(1)}(k+1|k) &= W_{d,j} \boldsymbol{\sigma}_{1,new}(k+1) \boldsymbol{\sigma}_{1,new}^T(k+1) + \\ &W_{d,c} \left(\sum_{j=1}^{2d} W_{d,j} \varphi^{-1}(\hat{\mathbf{x}}(k+1|k), \mathbf{x}_{\sigma_1}) \right) \left(\sum_{j=1}^{2d} W_{d,j} \varphi^{-1}(\hat{\mathbf{x}}(k+1|k), \mathbf{x}_{\sigma_1}) \right)^T \end{aligned} \quad (44)$$

$$\begin{aligned} P^{(2)}(k+1|k) &= W_{q,j} \boldsymbol{\sigma}_{2,new}(k+1) \boldsymbol{\sigma}_{2,new}^T(k+1) + \\ &W_{q,c} \left(\sum_{j=1}^{2q} W_{q,j} \varphi^{-1}(\hat{\mathbf{x}}(k+1|k), \mathbf{x}_{\sigma_2}) \right) \left(\sum_{j=1}^{2q} W_{q,j} \varphi^{-1}(\hat{\mathbf{x}}(k+1|k), \mathbf{x}_{\sigma_2}) \right)^T \end{aligned} \quad (45)$$

Correction: Once $\hat{\mathbf{x}}(k+1|k)$ and $P(k+1|k)$ are computed and the measurement $\mathbf{z}(k)$ is known, the correction can be performed. The sigma points are computed with the predicted state error covariance matrix as

$$\begin{aligned} \boldsymbol{\sigma}_{3,j}(k+1) &= \text{col}(\sqrt{(d+\lambda_d)P(k+1|k)})_j \quad j = 1, \dots, d \\ \boldsymbol{\sigma}_{3,j}(k+1) &= -\text{col}(\sqrt{(d+\lambda_d)P(k+1|k)})_{j-d} \quad j = d+1, \dots, 2d \end{aligned} \quad (46)$$

each of which is passed through the measurement function to compute the predicted measurement as

$$\begin{aligned} \hat{\mathbf{z}}_0 &= \mathbf{h}[\varphi(\hat{\mathbf{x}}(k+1|k), \mathbf{u}(k), t, 0)] \\ \hat{\mathbf{z}}_j &= \mathbf{h}[\varphi(\hat{\mathbf{x}}(k+1|k), \mathbf{u}(k), t, \boldsymbol{\sigma}_{3,j}(k+1))], \quad j = 1, \dots, 2d \\ \hat{\mathbf{z}}(k+1) &= W_{d,c} \hat{\mathbf{z}}_0 + \sum_{j=1}^{2d} W_{d,j} \hat{\mathbf{z}}_j \end{aligned} \quad (47)$$

and infer measurement covariance matrix $P_{\mathbf{zz}}$ and cross-covariance $P_{\mathbf{xz}}$ as

$$\begin{aligned} P_{\mathbf{zz}}(k+1|k) &= \sum_{j=0}^{2d} W_{d,j} (\hat{\mathbf{z}}_j - \hat{\mathbf{z}}(k+1)) (\hat{\mathbf{z}}_j - \hat{\mathbf{z}}(k+1))^T + R \\ P_{\mathbf{xz}}(k+1|k) &= \sum_{j=1}^{2d} W_{d,j} \boldsymbol{\sigma}_{3,j} (\hat{\mathbf{z}}_j - \hat{\mathbf{z}}(k+1))^T \end{aligned} \quad (48)$$

The Kalman gain is then given by

$$K(k+1) = P_{\mathbf{xz}}(k+1|k) P_{\mathbf{zz}}^{-1}(k+1|k) \quad (49)$$

Finally, the update can be obtained as

$$\begin{aligned} \hat{\mathbf{x}}(k+1|k+1) &= \varphi[\hat{\mathbf{x}}(k+1|k), K(k+1)(\mathbf{z}(k+1) - \hat{\mathbf{z}}(k+1))] \\ P(k+1|k+1) &= P(k+1|k) - K(k+1) P_{\mathbf{zz}}(k+1|k) K^T(k+1) \end{aligned} \quad (50)$$

The UKF filter performance is assessed through the accuracy and robustness of the algorithm. The accuracy index reflects the error in the estimated states, while the robustness refers to the capability of handling the

nonlinearities of the system. In a practical situation, the true states are not known in advance, and the accuracy is often evaluated with using the innovation sequence, which is defined as the difference between the actual measurements and the reconstructed states. The good performance of the UKF filter is confirmed through showing that the estimation error is bounded within the standard deviation envelopes. To elaborate, $\pm 2\sigma_\epsilon$ or $\pm 3\sigma_\epsilon$ are defined, where σ_ϵ represents the estimated standard deviation of the residual and is obtained from the diagonal elements of the state error covariance matrix P [34, 35]. Note that, although the technique discussed here is Jacobian-free, the UKF algorithm above is not globally stable due to the nonlinearities of the system, and, in order to guarantee the filter convergence, the estimated states should be selected to be initially close enough to the true states.

Tracking control

The control design in the SE(3) framework enables to treat both rotational and translational motions, simultaneously. The feedback loop allows to compute the difference between the desired configuration and the measured one, which is affected by the measurements errors. The controller should be able to nullify the error between the actual state and the desired state. The latter ones are computed by a guidance system, while the actual states come from the navigation filter, that has the main role of filtering out the measurement noises. Once the configuration error is defined, the controller can command the spacecraft translational and rotational motion through the actuators. An alternative asset could be the implementation of a controller robust to the uncertainties, i.e. a stochastic controller, without the use of a navigation system. In [36] the efficacy of such controller developed on SO(3) was shown. However, it is noted that for systems affected by different and high-magnitude sources of noise, the state can easily diverge if the stochasticity is not filtered out.

In this work two different types of tracking problem are considered: the hovering problem, where a tracking position with zero linear velocity is required, and the desired orbit problem, where a desired orbit around a small body is maintained. Moreover, a guidance logic is implemented to define the desired states. When the hovering problem is analyzed, a desired position in the inertial frame has to be selected. For the desired orbit mission, the desired position and velocity changes and are computed for each orbit point. In each instant of time the distance between the actual spacecraft position and all the points on the orbit is computed, then the closest point is located. If this point would be chosen as desired position, then the spacecraft would reach and keep it.

The guidance algorithm assigns the desired position \mathbf{r}_{ref} , velocity \mathbb{V}_{ref} , and attitude Θ_{ref} in combination with the actual states, to the control system. The UKF filter is used to obtain the estimated states $\hat{\mathbf{r}}$, $\hat{\mathbb{V}}$, and $\hat{\Theta}_{ref}$ in Eq. (51) from noisy measurements. The tracking errors can then be computed as

$$\begin{aligned}\epsilon_{R,track} &= R_{ref}^T(\Theta_{ref})R(\hat{\Theta}) \\ \epsilon_{\mathbf{r},track} &= \hat{\mathbf{r}} - \mathbf{r}_{ref} \\ \epsilon_{\mathbb{V},track} &= \hat{\mathbb{V}} - \mathbb{V}_{ref}\end{aligned}\tag{51}$$

The error dynamics in terms of position and velocity should tend to zero, and the rotation matrix to the identity matrix (i.e. null angles). Since the state is on TSE(3) and the control input is in \mathbb{R}^6 , different functions are introduced to allow the retraction from the manifold into the Euclidean space. The nonlinear function of the velocity and configuration is defined as

$$\psi(g_{err}, \epsilon_{\mathbb{V},track}) = \epsilon_{\mathbb{V},track} + K_1 \mathbf{I}(g_{err})\tag{52}$$

where $K_1 = \text{blockdiag}(k_{11}, k_{12}) \in \mathbb{R}^{6 \times 6}$ is a positive definite control gain matrix. The following function of the configuration is also introduced

$$\mathbf{I}(g) = [\mathbf{s}^T(\epsilon_{R,track}), \epsilon_{\mathbf{r},track}^T]^T\tag{53}$$

with its derivative

$$\dot{\mathbf{I}}(g_{err}) = [\dot{\mathbf{s}}^T(\epsilon_{R,track}), \mathbf{v}_{err}^T]^T\tag{54}$$

The $s(\cdot) : \text{SO}(3) \rightarrow \mathbb{R}^3$ and $\dot{s}(\cdot) : \text{SO}(3) \rightarrow \mathbb{R}^3$ are

$$\begin{aligned}\mathbf{s}(\boldsymbol{\epsilon}_{R,\text{track}}) &= \sum_{i=1}^3 a_i (\boldsymbol{\epsilon}_{R,\text{track}}^T e_i)^\times e_i = \sum_{i=1}^3 (\boldsymbol{\epsilon}_{R,\text{track}}^T A^T e_i)^x e_i \\ \dot{\mathbf{s}}(\boldsymbol{\epsilon}_{R,\text{track}}, \omega_{err}) &= (\text{tr}(A\boldsymbol{\epsilon}_{R,\text{track}})I_3 - \boldsymbol{\epsilon}_{R,\text{track}}^T A) \boldsymbol{\omega}_{err}\end{aligned}\quad (55)$$

where $e_i, i = 1, 2, 3$, are the elements of the natural basis in \mathbb{R}^3 , and $A = [\text{diag}(a_1, a_2, a_3)]$ with the scalars a_1, a_2 , and a_3 selected such that $a_1 > a_2 > a_3 \geq 1$. The control law developed for rigid body regulation control on TSE(3) in [9] is revised here to account for a tracking problem as

$$\mathbf{u}_c = -\mathbb{I}K_1\dot{\mathbf{i}} - \text{ad}_{\psi-K_1l}^*\mathbb{I}(\psi - K_1\mathbf{l}) - \mathbb{I}K_2\psi - \mathbb{I}\kappa [0_{1 \times 3}, \boldsymbol{\epsilon}_{r,\text{track}}^T \boldsymbol{\epsilon}_{R,\text{track}}^T]^T \quad (56)$$

where $K_2 = \text{blockdiag}(k_{21}, k_{22}) \in \mathbb{R}^{6 \times 6}$ is a positive definite control gain matrix, and k_{21} and k_{22} can be tuned suitably to adjust rotation and translation performance of the spacecraft. Thus, the total augmented control input is $\mathbf{u}_c = [\mathbf{F}_c^T, \mathbf{M}_c^T]^T$, as defined in Eq. (11). According to [9], the backstepping approach guarantees the convergence. Lyapunov stability analysis of the controller on TSE(3) for the rigid body regulation problem given in [9] also guarantees the almost global asymptotic stability of the tracking problem studied here.

According to [37], the separation principle allows the design of the controller and the observer (filter algorithm) separately. Particularly, if the observer and the controller are both stable, then the closed-loop dynamics obtained using the augmentation of them is also stable. In many applications, this technique has proved to be a successful and stable design method. In order to highlight the different type of errors, the tracking errors in Eq. (51) are rewritten as

$$\begin{aligned}\boldsymbol{\epsilon}_R &= R_{ref}^T(\boldsymbol{\Theta}_{ref})\hat{R}(\hat{\boldsymbol{\Theta}})\hat{R}^T(\hat{\boldsymbol{\Theta}})R(\boldsymbol{\Theta}) = \boldsymbol{\epsilon}_{R,\text{track}}\boldsymbol{\epsilon}_{R,\text{est}} \\ \boldsymbol{\epsilon}_r &= \mathbf{r} - \hat{\mathbf{r}} + \hat{\mathbf{r}} - \mathbf{r}_{ref} = \boldsymbol{\epsilon}_{r,\text{est}} + \boldsymbol{\epsilon}_{r,\text{track}} \\ \boldsymbol{\epsilon}_v &= \mathbb{V} - \hat{\mathbb{V}} + \hat{\mathbb{V}} - \mathbb{V}_{ref} = \boldsymbol{\epsilon}_{v,\text{est}} + \boldsymbol{\epsilon}_{v,\text{track}}\end{aligned}\quad (57)$$

where $\boldsymbol{\epsilon}_{\text{est}}$ and $\boldsymbol{\epsilon}_{\text{track}}$ denote the estimation error and the tracking error, respectively. According to Eq. (57), when the estimation error and tracking error go to zero, the total error goes to zero, meaning that both the estimator and controller are asymptotically stable (in addition, the controller is almost globally asymptotically stable⁹). The convergence of the controller results in a zero tracking error, and the convergence of the filter results in a bounded estimation error, with zero mean white noise.

NUMERICAL SIMULATIONS AND DISCUSSION

This section presents the results obtained with the implementation of the introduced techniques on TSE(3). The dynamics of the system are propagated using the variational integrator directly on the nonlinear manifold SE(3), where the discretized Hamiltonian is used. Variational integrator used here is advantagous over conventional Runge-Kutta integrator since it preserves the geometric properties of the system [38, 39].

In order to show the performance of the proposed navigation and control scheme, two case studies are considered, and the spacecraft motion is studied with respect to the body frame of the celestial object in both cases. Three different quantities are analyzed: (i) the measured states which represent the state variables measured by sensors and hence are affected by noise, (ii) the filtered states which are the outputs of the navigation system, and (iii) the ideal states which are the noise-free states obtained with ideal and perfect sensors.

Case Study 1: Desired Orbit Problem Around Pan

In the first scenario, the small irregular Saturnian moon Pan is considered. Its orbit is nearly circular and it is tidally locked with Saturn, orbiting once every ~ 14 hours and thus spinning beneath the spacecraft once every orbit. Hence $\omega_p = 1.2643 \times 10^{-4} \frac{\text{rad}}{\text{s}}$. Pan is a non spherical object with an estimated $C_{20} = -3.7249 \times 10^{-4}$

km^2 and $C_{22} = 2.8193 \times 10^{-5}$, based on Cassini observational data which places the estimated dimensions of the object of $34.4 \times 31.4 \times 20.8 \text{ km}$ [40]. The mass of Pan is estimated to be $(4.95 \pm 0.75) \times 10^{15} \text{ kg}$, and thus the gravitational parameter μ_p is approximated at $3.793 \times 10^{-4} \frac{\text{km}^3}{\text{s}^2}$.

Table 1. Initial conditions and control parameters of the spacecraft for the desired orbit problem around Pan.

spacecraft properties and initial conditions	
$\mathbf{r}_0 = [65, 10, 15]^T \text{ km}$	$\mathbf{v}_0 = \sqrt{\frac{\mu}{ \mathbf{r}_0 }} [0.4, 1, 0]^T \text{ km/s}$
$\Theta_0 = [90, 90, -90]^T \text{ deg}$	$\omega_0 = [15, 3, 9]^T \text{ deg/s}$
$m = 60 \text{ kg}$	$J = \text{diag}(4.97, 6.16, 8.37) \text{ kgm}^2$
controller	
$\kappa = 0.002$	$k_{11} = 0.2$
$k_{12} = 0.1$	$k_{21} = 1.0$
$k_{22} = 0.01$	$A = \text{diag}(1.2, 1.1, 1.0) \text{ kgm}^2$
noise statistics	
$\sigma_{\zeta_r} = 0.1 \text{ km}$	$\sigma_{\eta_r} = 0.001 \text{ km}$
$\sigma_{\zeta_v} = 0.2 \text{ km/s}$	$\sigma_{\eta_v} = 0.01 \text{ km/s}$
$\sigma_{\zeta_\Theta} = 28.65 \text{ deg}$	$\sigma_{\eta_\Theta} = 0.0572 \text{ deg}$
$\sigma_{\zeta_\omega} = 11.5 \text{ deg/s}$	$\sigma_{\eta_\omega} = 0.573 \text{ deg/s}$
desired orbit	
$a_{ref} = 70.7 \text{ km}$	$e_{ref} = 10^{-3}$
$i_{ref} = 25 \text{ deg}$	$\Omega_{ref} = 0 \text{ deg}$
$\omega_{ref} = 0 \text{ deg}$	$l_{ref} = 0 \text{ deg}$
$\Pi_{ref} = 0 \text{ deg}$	$u = 0 \text{ deg}$
desired attitude	
$\Theta_{ref} = [12, 5, 9]^T \text{ deg}$	$\omega_{ref} = [0, 0, 0]^T \text{ deg/s}$

The spacecraft parameters and initial conditions, the assumptions for the controller gains values, noise statistics, and desired orbit Keplerian elements are given in Table 1, where the spacecraft mass and inertia are chosen for a small spacecraft. The initial tracking error is different from zero, so the spacecraft has an initial tumbling. In a similar way, the noise standard deviations are considered high, to show the performance of the navigation system. The near-circular desired orbit is inclined and has a semi-major axis slightly larger than twice the Pan's radii.

In Fig. 1, the trajectory of the center of mass of spacecraft and the desired orbit are shown. The spacecraft state is represented by the filtered state, obtained with the implementation of both the navigation and control system. Therefore, as can be seen in the figure, the spacecraft estimated trajectory (and states) approaches the desired orbit (and states), and hence indicating the convergence in the system. In Fig. 2 the measured-, filtered-, and ideal states are represented. The measurements are extremely noisy since the variances are selected to be high. For instance, the angular velocity components approach zero once the spacecraft is in the orbit, but the sensors measure the angular velocity to be in the range of $\pm 8 \text{ deg}$ which is a large range. It is clear that the navigation system, which is based on the UKF algorithm, is capable of estimating all the states with high accuracy and converges in less than 100 s. Then, the filtered states at each time step are used in the controller.

It is clear from Figs. 1 and 2 that the control system is capable of bringing the spacecraft to the desired orbit within a reasonably small amount of time while also maintaining its motion in the orbit. The position and linear velocity, after a small transient response, have smooth oscillatory behavior as they evolve in time. This behavior is expected since the spacecraft is maintaining its orbit around Pan. The desired Euler angles and

angular velocity of the spacecraft are reported in Table 1. In Fig. 3 (first two plots) the estimated state error between the filtered and the ideal states are shown along with the confidence bounds of $3\sigma_\epsilon$. As highlighted in the UKF design section, the optimal performance of the estimator is indicated by the bounded estimation error within the variance bounds. Finally, the control inputs are reported in the last plot in Fig. 3. It can be seen in that figure that the force and moment control inputs reach a peak of 8 kN and -2 kNm, respectively. These relatively high control inputs are due to the fact that the spacecraft is assumed to be initially tumbling at a relatively high rate and since it is initially out of the orbit by a large margin. Another reason for this is that the filter has not perfectly converged up to that point.

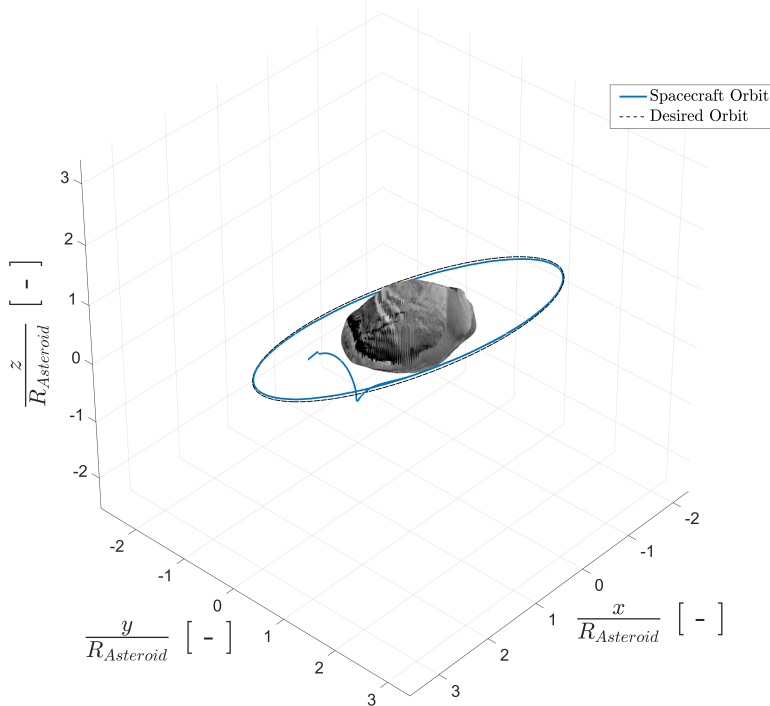


Figure 1. Spacecraft orbit (blue) around Pan, obtained via simultaneous implementation of the filter and control on the noisy measurements vs. the desired orbit in (black).

Case Study 2: Hovering Around Asteroid Bennu

The second scenario is an hovering maneuver around asteroid Bennu, which is a more well-understood body than Pan. Since the publication of the work [18], this near-Earth object has been visited by OSIRIS-REx and thus more accurate estimates of its mass and size have been obtained. A gravitational parameter of $5.2 \times 10^{-9} \text{ km}^3/\text{s}^2$ is used based on a mass of $(7.329 \pm 0.009) \times 10^{10} \text{ kg}$. The dimensions of Bennu are $(l_1, l_2, l_3) = (365, 535, 508) \text{ km}$, resulting in a $C_{20} = -0.3506$ and $C_{22} = 0.06477$, respectively. The larger dimensions of Bennu with respect to Pan are manifested by the higher values of the dimensionless coefficients C_{20} and C_{22} .

The spacecraft properties and initial conditions, controller gains values, noise statistics and desired orbit Keplerian elements are considered as in Table 2. The same spacecraft (with the same mass and inertia properties) and same sensor statistics as in the previous case study are considered here. However, the controller gains have been tuned differently from the previous case in order to obtain the desired motion for this new scenario. As can be seen from the relatively large values of the initial angular velocity, it is assumed that the vehicle is initially highly tumbling.

In Fig. 4 (first plot), the spacecraft trajectory is shown along with the the desired position in the space.

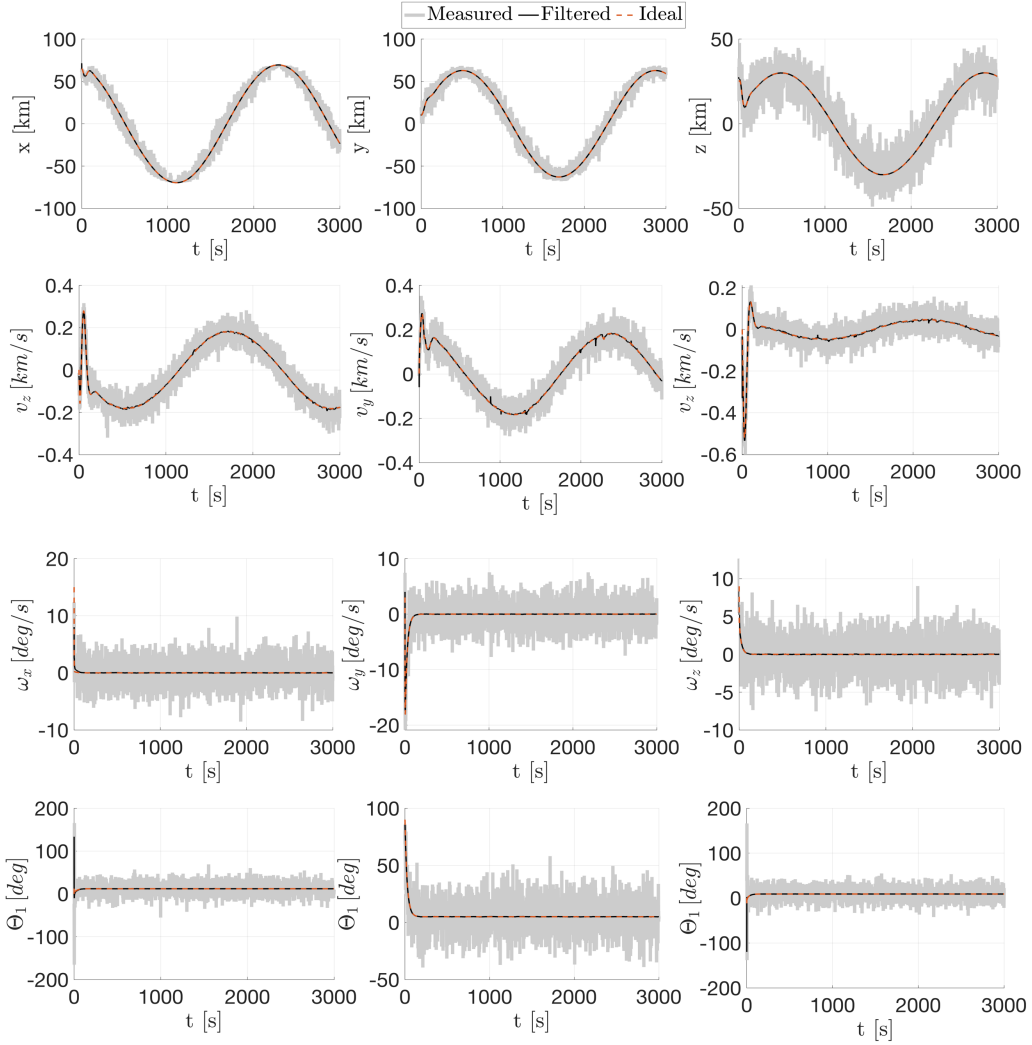


Figure 2. Measured (grey), filtered (black) and ideal (red) states.

The blue line in the figure is obtained by applying the navigation and control algorithm to the system. The transient response of the system can be improved by further tuning the controller parameters. In Fig. 4 (second and third plot), the measurements, the filtered/estimated states, and the ideal ones are reported. The noisy measurements could make the system diverge due to the incorrect computation of the tracking error. However, the good performance of the navigation system makes the filtered state to converge to the ideal states in about 20 – 50 s. It can be seen in this figure that the spacecraft states converge to the desired values in less than 100 s. Note that this case study considers the spacecraft hovering at a fixed position above the asteroid, where the spacecraft is guided into a stationary point above the surface of Bennu and remains at that point. Figure 5 (first and second plot) depicts the state estimation error which is well bounded within the $3\sigma_\epsilon$ envelopes, thus indicating the efficiency of the UKF. It can be seen that in this case the bounds reaches a steady value, while in the desired orbit problem they were oscillating. Finally, the control inputs are shown in Fig. 5 (last plot). In this case the control force and moment are highly higher than the previous case, since the gains have been tuned to guarantee a faster convergence. With increasing the settling time, the control inputs can be reduced, decreasing the controller gains.

Table 2. Initial conditions and control parameters for the hovering problem around Bennu

spacecraft properties and initial conditions	
$\mathbf{r}_0 = [1.6, -1.3, -1]^T \text{ km}$	$\mathbf{v}_0 = \sqrt{\frac{\mu}{ \mathbf{r}_0 }}[0.3, 1, 0.1]^T \text{ km/s}$
$\Theta_0 = [-30, -25, 18]^T \text{ deg}$	$\boldsymbol{\omega}_0 = [115, 60, 96]^T \text{ deg/s}$
$m = 60 \text{ kg}$	$J = \text{diag}(4.97, 6.16, 8.37) \text{ kgm}^2$
controller	
$\kappa = 0.001$	$k_{11} = 0.2$
$k_{12} = 1.0$	$k_{21} = 1.0$
$k_{22} = 0.1$	$A = \text{diag}(1.2, 1.1, 1.0) \text{ kgm}^2$
noise statistics	
$\sigma_{\zeta_r} = 0.1 \text{ km}$	$\sigma_{\eta_r} = 0.001 \text{ km}$
$\sigma_{\zeta_v} = 0.2 \text{ km/s}$	$\sigma_{\eta_v} = 0.01 \text{ km/s}$
$\sigma_{\zeta_\Theta} = 28.65 \text{ deg}$	$\sigma_{\eta_\Theta} = 0.0572 \text{ deg}$
$\sigma_{\zeta_\omega} = 11.5 \text{ deg/s}$	$\sigma_{\eta_\omega} = 0.573 \text{ deg/s}$
desired position	
$\mathbf{r}_{ref} = [-1.5, 1, 0.5]^T \text{ km}$	$\mathbf{v}_{ref} = [0, 0, 0]^T \text{ km/s}$
desired attitude	
$\Theta_{ref} = [30, 20, 10]^T \text{ deg}$	$\boldsymbol{\omega}_{ref} = [0, 0, 0]^T \text{ deg/s}$

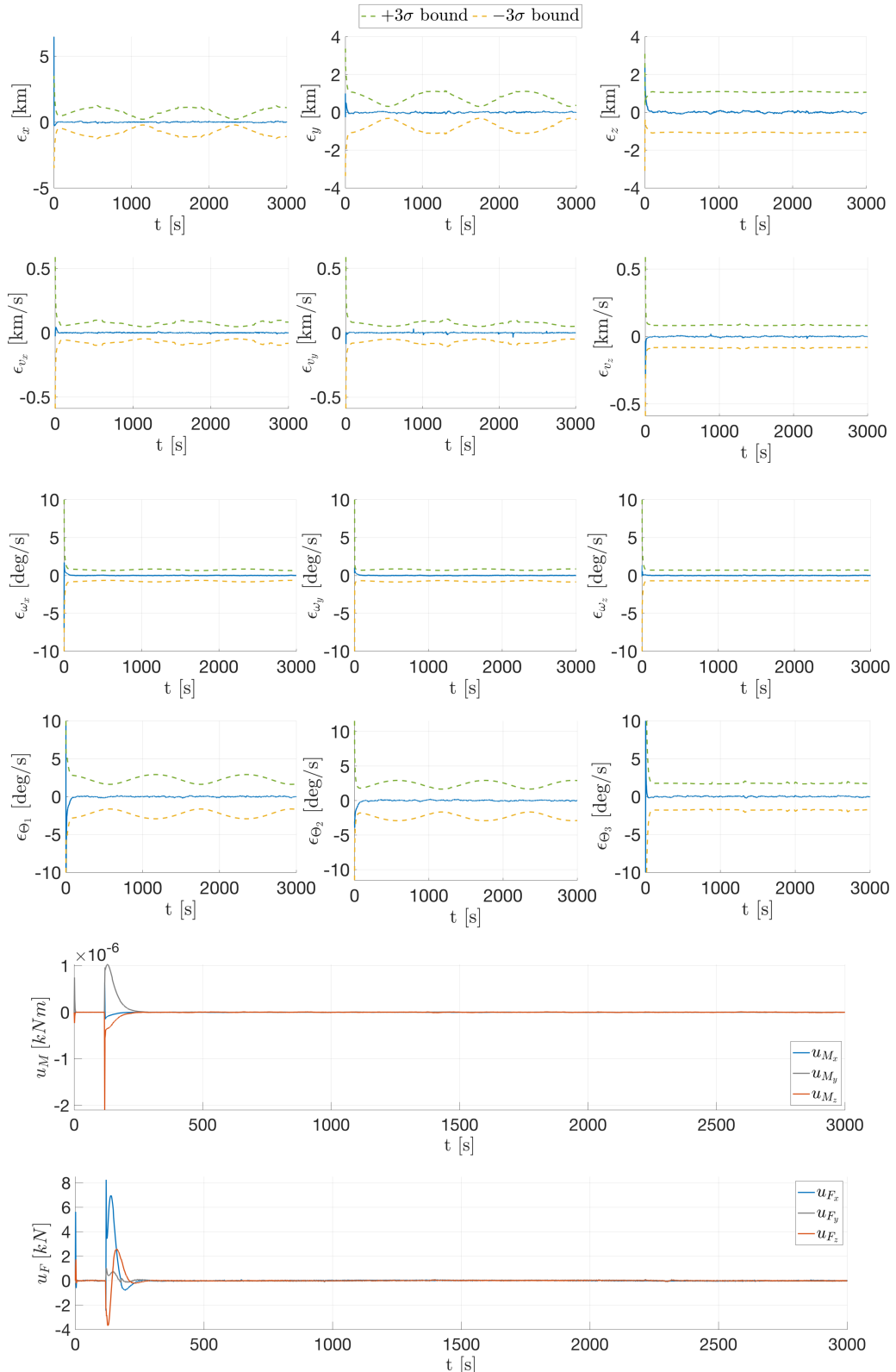


Figure 3. State estimation error between the estimated (filtered) and the ideal noise-free states (first two plots) and the history of the control force and moment components (bottom).

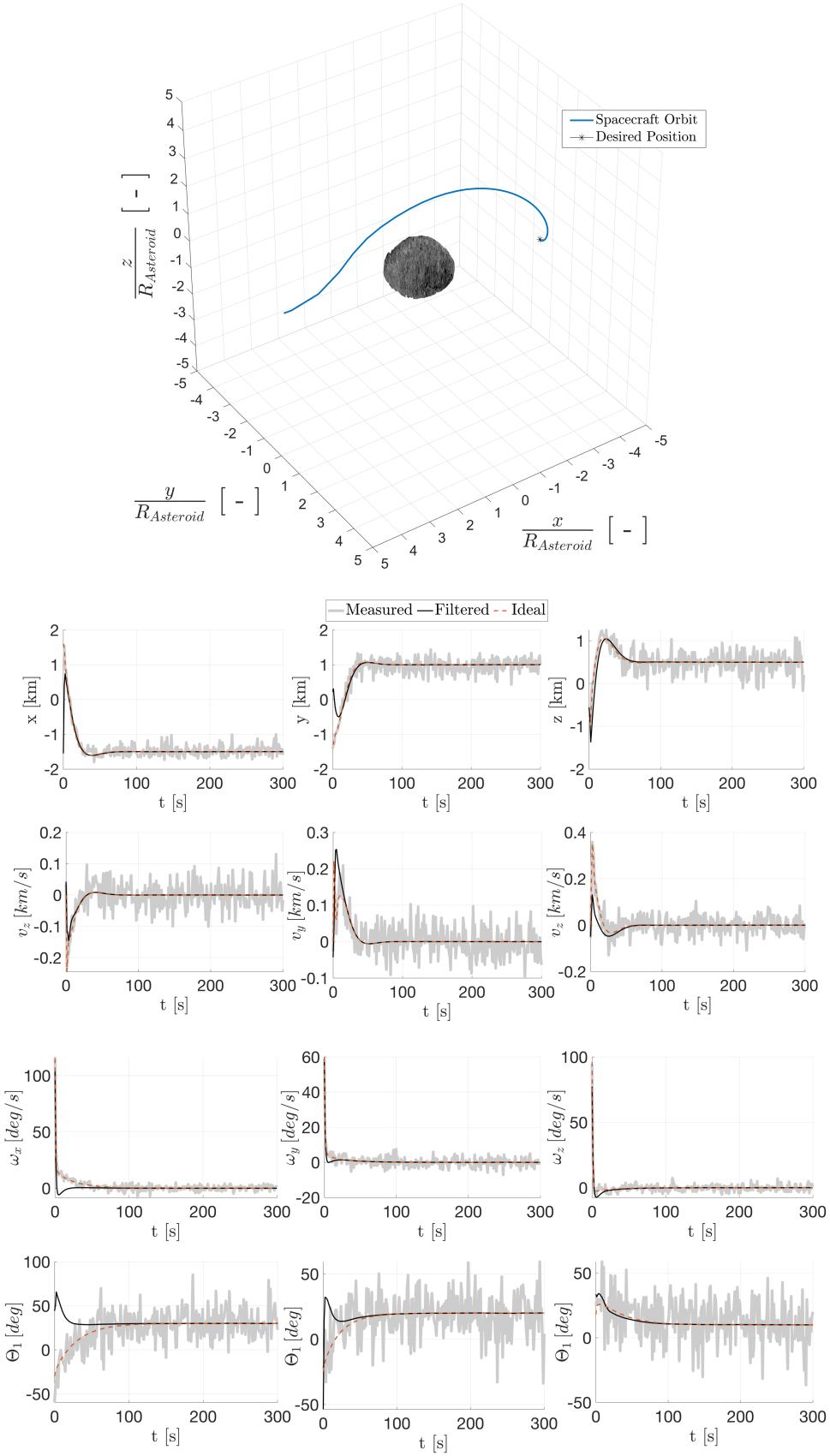


Figure 4. Spacecraft orbit (blue) around Bennu, obtained via simultaneous implementation of the filter and control on the noisy measurements vs. the desired orbit (black) (3-D). Measured (grey), filtered (black) and ideal (red) states (bottom plots).

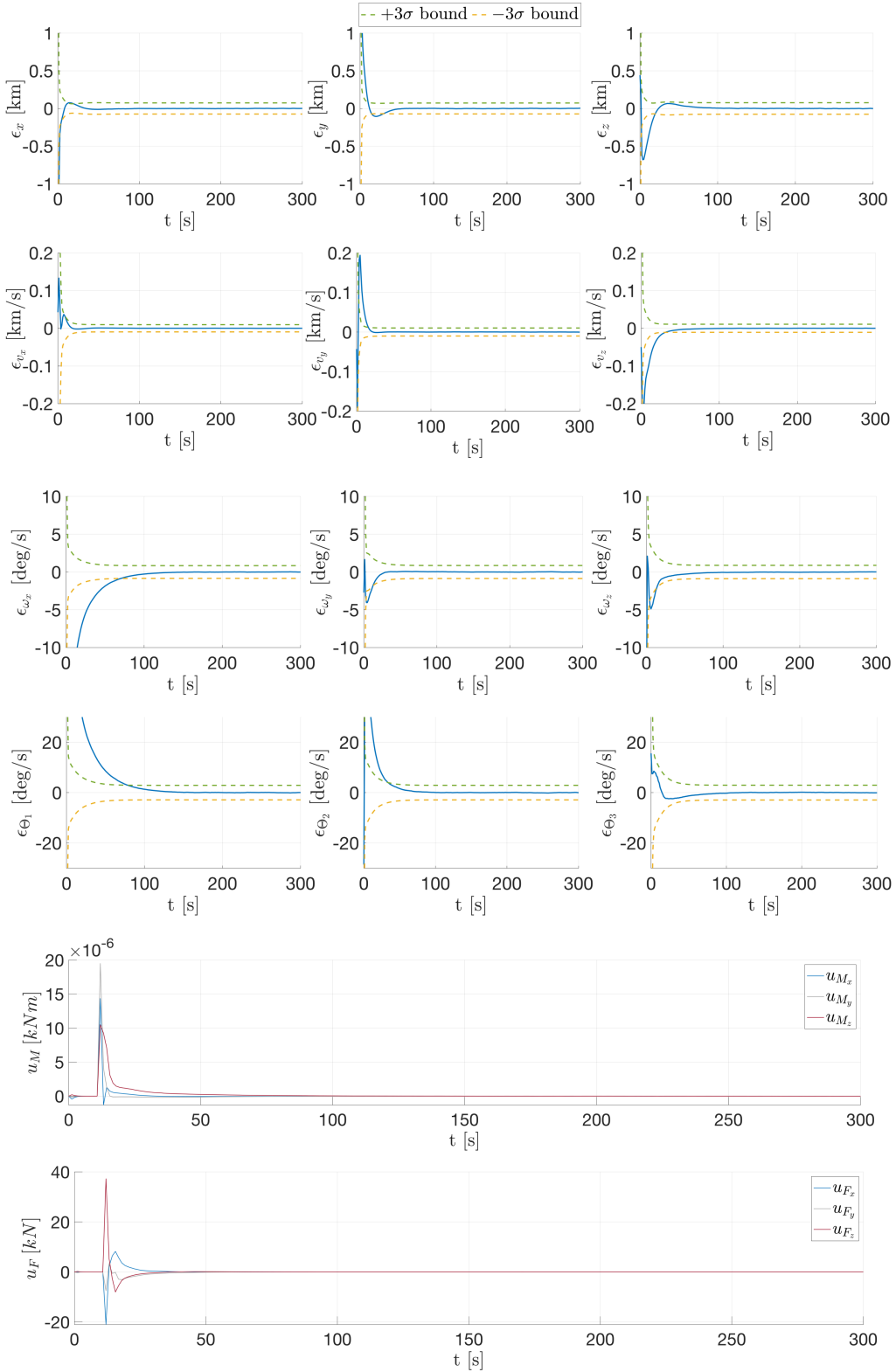


Figure 5. State estimation error between the estimated (filtered) and the ideal noise-free states (first two plots). The history of the control force and moment components (bottom).

CONCLUSIONS AND FUTURE WORK

In this work, a novel spacecraft navigation and control system has been developed in the Lie group $SE(3)$ and its tangent bundle $TSE(3)$ in the presence of stochastic processes in the system. In the mathematical framework presented here, the geometrical system characteristics are well preserved and the translational and attitude motions are treated simultaneously. Hence, this formalism allows for the coupling between orbital and attitude motions of the spacecraft to be accounted for. This coupling cannot be neglected in the rigid-body spacecraft motion scenarios around small irregular celestial bodies, due to their highly perturbed environments. The estimated results obtained using an unscented Kalman filter on $TSE(3)$ are used in a Lyapunov-Morse-based feedback control with backstepping law to estimate and control the system states with noisy measurements. The methodology used here is to prove that the augmentation of the stochastic estimation, control, and dynamics in $TSE(3)$ provides a reliable, functional method of guidance and navigation around small irregular bodies. The numerical results, confirming the theoretical expectations, showed that the navigation and control system presented here is capable of conducting the spacecraft towards a desired orbit or position in the space.

As a future work, the robustness of the stochastic estimation and control scheme presented in this work can be tested in problems such as multi-body dynamics, orbit transfers, spacecraft rendezvous, or proximity operations and docking. The results presented in this work can be improved by considering the presence of solar radiation pressure or spherical harmonics of orders higher than C_{20} and C_{22} in the dynamic modeling. Furthermore, the results presented in this work are obtained using a simple logic since the logic design was out of the scope of this work. Hence, another relevant improvement can be through the implementation of a guidance system for the orbit tracking problem that is more robust than the one presented here.

ACKNOWLEDGMENT

Support from Faculty Innovative Research in Science and Technology (FIRST) is gratefully acknowledged. Some of the MATLAB scripts used in this project are based on the work of Julio Benavides, now at Odyssey Space Research, whose well-commented and documented work has long been helpful.

REFERENCES

- [1] K. R. Pollock, *An analysis of orbital propagators for low earth orbit rendezvous*. 1994.
- [2] S. P. Shuster, *A Survey and Performance Analysis of Orbit Propagators for LEO, GEO, and Highly Elliptical Orbits*. All Graduate Theses and Dissertations, 2017.
- [3] V. Vittaldev, E. Mooij, and M. C. Naeije, *Unified state model theory and application in Astrodynamics*. Celestial Mechanics and Dynamical Astronomy, 2012.
- [4] F. L. Markley and J. L. Junkins, *Fundamentals of spacecraft attitude determination and control*. Springer, 2014.
- [5] H. Schaub and J. L. Junkins, *Analytical Mechanics Of Space Systems*. American Institute of Aeronautics and Astronautics, 2018.
- [6] W. Fehse, *Automated rendezvous and docking of spacecraft*. Cambridge university press, Cambridge, 2003.
- [7] M. J. Sidi, *Spacecraft Dynamics and Control: A Practical Engineering Approach*. Cambridge University Press, Cambridge, 1997.
- [8] D. Lee and G. Vukovich, *Robust Adaptive Terminal Sliding Mode Control on $SE(3)$ for Autonomous Spacecraft Rendezvous and Docking*. Nonlinear Dynamics, 2016.
- [9] M. Nazari, M. Maadani, E. A. Butcher, and T. Yucelen, *Morse-Lyapunov-Based Control of Rigid Body Motion on $TSE(3)$ via Backstepping*. 2018.
- [10] D. Seo and M. Nazari, *Rigid Body Adaptive Stabilization on the Tangent Bundle of the LIE Groups*. AIAA GNC Conference, 2019.
- [11] Y. W. L. Jiang and S. Xu, *Integrated 6-DOF Orbit-Attitude Dynamical Modeling and Control Using Geometric Mechanics*. International Journal of Aerospace Engineering, 2017.
- [12] K. Gong, Y. Liao, and Y. Wang, *Adaptive Fixed-Time Terminal Sliding Mode Control on $SE(3)$ for Coupled Spacecraft Tracking Maneuver*. International Journal of Aerospace Engineering, 2020.
- [13] G. Bourmaud, R. Megret, A. Giremus, and Y. Berthoumieu, *Discrete Extended Kalman Filter on Lie Groups*. 21st European Signal Processing Conference, 2013.

- [14] M. Brossard, S. Bonnabel, and J. Condomines, *Unscented Kalman filtering on Lie groups*. IEEE/RSJ International Conference on Intelligent Robots and Systems (IROS), 2017.
- [15] M. Brossard, S. Bonnabel, and A. Barrau, *Unscented Kalman Filter on Lie Groups for Visual Inertial Odometry*. IEEE/RSJ International Conference on Intelligent Robots and Systems (IROS), 2018.
- [16] G. Loianno, M. Watterson, and V. Kumar, *Visual Inertial Odometry for Quadrotors on SE(3)*. IEEE International Conference on Robotics and Automation (ICRA), 2016.
- [17] G. Bourmaud, R. Megret, and A. G. M. Arnauden, *Continuous-Discrete Extended Kalman Filter on Matrix Lie Groups Using Concentrated Gaussian Distributions*. Springer, 2014.
- [18] G. Misra, A. Sanyal, and D. J. Scheeres, *Coupled orbit-attitude dynamics and relative state estimation of spacecraft near small solar system bodies*. Advances in Space Research, 2015.
- [19] M. Brossard, A. Barrau, Axel, and S. Bonnabel, *A Code for Unscented Kalman Filtering on Manifolds (UKF-M)*. International Conference on Robotics and Automation (ICRA), 2020.
- [20] A. Muller and Z. Terze, *The significance of the configuration space Lie group for the constraint satisfaction in numerical time integration of multi body systems*. Mechanism and Machine Theor, 2014.
- [21] T. Lee, H. Mcclamroch, and M. Leok, *Optimal Attitude Control for a Rigid Body with Symmetry*. Proceedings of the American Control Conference, 2007.
- [22] J. Sola, J. Deray, and D. Atchuthan, *A micro Lie theory for state estimation in robotics*. 2018.
- [23] R. M. Murray, Z. Li, and S. S. Sastry, *A Mathematical Introduction to Robotic Manipulation*. CRC Press, 1994.
- [24] J. Gallier, *Basics of Classical Lie Groups: The Exponential Map, Lie Groups, and Lie Algebras, In: Geometric Methods and Applications*. Texts in Applied Mathematics, vol 38. Springer.
- [25] M.-A. A. H. Ahmed, *On Extracting Properties of Lie Groups from Their Lie Algebras*. American Journal of Computational and Applied Mathematics, 2016.
- [26] M. Nazari, E. A. Butcher, T. Yucelen, and A. Sanyal, *Decentralized Consensus Control of a Rigid-Body Spacecraft Formation with Communication Delay*. Journal of Guidance, Control, and Dynamics, 2016.
- [27] D. J. Scheeres, *Orbital Motion in Strongly Perturbed Environments*. Springer,Berlin-Heidelberg, 2012.
- [28] W. M. Kaula, *Theory of Satellite Geodesy*. Blaisdell, Bosto, 1966.
- [29] D. J. Scheeres, S. J. Ostro, R. S. Hudson, E. M. DeJong, and S. Suzuki, *Dynamics of orbits close to asteroid 4179 Toutatis*. 1998.
- [30] M. Nazari, R. Wauson, T. Critz, E. A. Butcher, and D. J. Scheeres, *Observer-based body-frame hovering control over a tumbling asteroid*. Acta Astronautica, 2014.
- [31] T. D. Barfoot and P. T. Furgale, *Associating Uncertainty With Three-Dimensional Poses for Use in Estimation Problems*. IEEE Transactions on Robotics, 2014.
- [32] J. A. Mulder, J. K. S. Q. P. Chu, J. H. Breeman, and M. Laban, *Non-linear aircraft flight path reconstruction review and new advances*. Progress in Aerospace Sciences, 1999.
- [33] E. A. Wan and R. V. D. Merwe, *The unscented Kalman filter for nonlinear estimation*. Proceedings of the IEEE 2000 Adaptive Systems for Signal Processing, Communications, and Control Symposium, 2000.
- [34] I. Miletović, D. Pool, O. Stroosma, M. M. V. Paassen, and Q. Chu, *Improved Stewart platform state estimation using inertial and actuator position measurements*. Control Engineering Practice, 2017.
- [35] J. B. Moor and B. D. O. Anderson, *Optimal Filtering*. Prentice Hall Information and System Sciences Series, 1979.
- [36] E. Samiei, M. Nazari, and E. A. B. A. K. Sanyal, *Robust stochastic stabilization of attitude motion*. International Journal of Dynamics and Control, 2019.
- [37] K. K. Tønne, “Stability analysis of ekf - based attitude determination and control,” 2007.
- [38] T. Lee, M. Leok, and N. Mcclamroch, “Lie group variational integrators for the full body problem,” *Computer Methods in Applied Mechanics and Engineering*, vol. 196, 08 2005.
- [39] J. Marsden and M. West, *Discrete mechanics and variational integrators*. Acta Numerica 10, 2001.
- [40] P. Thomas, *Sizes, shapes, and derived properties of the saturnian satellites after the Cassini nominal mission*. Icarus, Volume 208, Issue 1, July 2010, pp 395-401, 2010.